The International Congress of Immunology 2016, August 21-26, 2016, Melbourne

Immunogenicity of M13 phage vaccine displaying N-terminal region of amyloid beta peptide: comparison of M13 phage vaccine expressed as g3p fusion and g8p fusion.

Ryuji Miyahara[1], Akiko Shimotsu[1], Yui Matsushita[1], Taisuke Shinozaki[1], Mai Tsukada[1], Masahito Hashimoto[1], Kazuhisa Sugimura[2], Shuhei Hashiguchi[1]

Abstract

Antibodies against amyloid-ß peptide (Aß) can reduce amyloid deposits and are considered as a potential therapeutic approach for Alzheimer's disease[1,2]. We have recently shown that M13 phage stimulate an innate immune response and induce a strong primary IgG response in mice without any inflammatory adjuvant materials[3,4]. Even a single immunization with 10^{11} pfu of phage induced a long-lasting antibody response. To investigate the potential of M13 phage as a vaccine carrier for Aß peptide, the sequences of 1-15 region of Aß were genetically linked to the N-terminus of M13 gene 3 protein or gene 8 protein, that correspond to Aß-g3p phage and Aß-g8p phage, respectively. When C57BL/6 mice were immunized subcutaneously with 10^{11} pfu of Aß-g3p phage in PBS solution, anti-Aβ IgG response was induced in two weeks after the secondary immunization. In the case of Aβ-g8p phage, anti-Aß IgG response was induced during a primary response. Anti-Aß antibody titer was comparable in the two mice groups. We also observed that Aβ-g8p phage induced IgG class switch in athymic (nu/nu) BALB/c mice, indicating that there are different immunological mechanisms of phage vaccine between g3p fusion and g8p fusion. Considering safety and habitual presence of an M13 phage, Aß1-15-displaying M13 phage may be promising as a safe AD vaccine.

References

1) Schenk D, et al. Nature, 400, 173-177, (1999).

2) Bard F, et al. Nat Med, 6, 916-919, (2000).

3) Hashiguchi S, et al. Biochem Biophys Res Commun,402, 19-22, (2010).

4) Tanaka K, et al, J.Neuroimmunol, 236, 27-38, (2011).

[1]Graduate School of Science and Engineering, Kagoshima University, Kagoshima, Japan

[2]Graduate School of Medical and Dental Sciences, Kagoshima University, Kagoshima, Japan

The 42nd Annual Conference of the IEEE Industrial Electronics Society, October 23-26, 2016,
Palazzo dei Congressi, Florence, Italy

Finite-Time Stabilization of Ultrasonic Motor With Stochastic Compensator for Chattering Phenomena

Hiroyuki YOSHINO*, Yûki NISHIMURA* and Kanya TANAKA**

Abstract

Ultrasonic motors are attracting attention because of having characteristics such as high-torque in low-speed, high responsively and electromagnetic compatibility. However, they have strong nonlinearity because of having frictions as driving sources generated by piezoelectric effects and having the dynamics changing depending on temperature of the motors. Those physical characteristics cause the difficulty of deriving mathematical models and control laws [1]. This motivates constructing simple mathematical models and simple controllers having a robustness property for modeling errors. In this direction, the servo control problems are investigated in [2]. Because the investigations imply that we should, absolutely, allow the system models having nonlinearity between the input and the output, a positioning control system is derived based on a state-space model with considering the nonlinearity in [3]. To develop the controller so that they have further rapid stabilization and further precise settling accuracy, we consider employing the concept of finite-time stabilization. However, in theory, the finite-time convergence property results in discontinuous phenomena when just achieving the target position. This yields that, in practical experiments, chattering-like phenomena occur about the target position [4] as with sliding mode controls. Because the phenomena are obstacles for precise controls, we should attenuate them by providing compensators. In this paper, we propose a new compensator for the chattering-like phenomena by dealing with them as Gaussian white noises appearing about the target position only. This treatment enables us to employ stochastic stability analysis [5]; that is, we can evaluate the effects of the compensator by theoretical analysis while the phenomena appear in practical experiments only. Furthermore, the compensator keeps finite-time convergence to the target points different from adding time intervals of no control (dead time).

References

[1] N. W. Hagood IV and A. J. McFarland: Modeling of a piezoelectric rotary ultrasonic motor, IEEE Transactions on Ultrasonics, Ferroelectrics, and Frequency control, 42-2, 210/224, 1995.
[2] F.A. Rahman, Y. Murata, K. Tanaka, Y. Nishimura, S. Uchikado, and Y. Osa: Variable gain type PID control using PSO for ultrasonic motor; Proc. 5th International Workshop on Computational Intelligence & Applications IEEE SMC Hiroshima Chapter, 2009.
[3] Y. Nishimura, K. Tanaka, Y. Wakasa and H. Nakamura: Robust angle regulation for ultrasonic motor using CLF-based controller; Proc. IECON 2011, 2011.
[4] Y. Nishimura, H. Yoshino and K. Tanaka: Positioning control of ultrasonic motor using homogeneous finite-time control, Transactions of The Institute of Systems, Control and Information Engineers, 29-6, 235/241, 2016 (in Japanese).
[5] R. Z. Khasminskii. Stochastic Stability of Differential Equations, Second Edition, Springer, 2012.

*Department of Mechanical Engineering, Graduate School of Science and Engineering, Kagoshima University, **Department of Electrical and Electronic Engineering, Graduate School of Science and Engineering, Yamaguchi University

International Association for Shell and Spatial Structures (IASS) Symposium 2016,
September 26-30, 2016, Tokyo, Japan

Shape Optimization by Presence of Antiplane Shear Deformation in Free-Form Shell Structure

Tetsuro Nishida[1], Toshio Honma[1] and Yohei Yokosuka[1]

Abstract

In this study, we investigate a difference of forms obtained by shape optimization using shell element with/without the antiplane shear deformation for free-form shell structures. Free-form shell structures with a long span are designed many practical projects recently. Such structural systems need to satisfy both designability and mechanical rationality. However, a decision of a curved shape for the free-form shell structure by a designer's experience and intuition is difficult. In the shape optimization computation using the coordinates of curved surface and the shell thickness as design variables, the influence that receives stress concentration is different according to the type of the support condition. Therefore, the support neighborhood tends to make the shell thickness thick by the shape optimization [1], and in the computation that uses the shell element (finite element) without the antiplane shear deformation (Kirchhoff-Love theory) [2], there is a possibility of not indicating a correct stress state.

In this paper, we indicate the difference of numerical solutions for shell element based on Kirchhoff-Love theory and Mindlin-Reissner theory [3] using a support with stress concentration in an analysis model of a shape optimization. Next, we apply a support condition of easing the stress concentration in the analysis model. The solution search approach of shape optimization adopts Artificial Bee Colony (ABC) [4] that is one of the heuristic procedures. The figures below are an example of the numerical result by the shape optimization using shell element with/without the antiplane shear deformation.

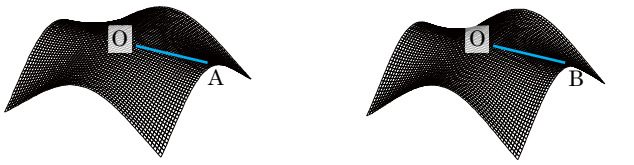

a. by Kirchhoff-Love theory　　b. by Mindlin-Reissner theory

Figure. Solution forms

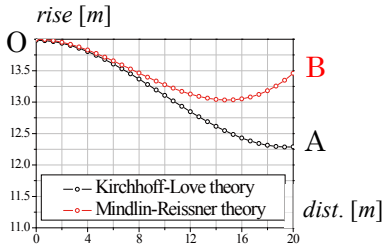

Figure. Cross-sectional shape (━)

References

1. K. Nagata and T. Honma, Structural Morphogenesis for Free Form Surface Shell Using Swarm Intelligence with Decent Solution Search Manipulation, CD-ROM Proc. Of 7th China-Japan-Korea Joint Symposium on Optimization of Structural and Mechanical Systems, 2012.
2. O.C.Zienkiewicz, R.L. Taylor, The Finite Element Method, 5th edition. Vol.2, Butterworth-Heinemann, 2000.
3. K.J.Bathe and E.N.Dvorkin: Short communication a four-node plate bending element based on Mindlin/Reissner plate theory and a mixed interpolation, Vol.21, 367-383, 1985.
4. D.karaboga and B.Basturk: A powerful and efficient algorithm for numerical function optimization; artificial bee colony (ABC) algorithm, Journal of Golb Optimization 39,459-471, 2007.

[1] Department of Architecture &Architectural Engineering, Kagoshima University, 890-0065, Kagoshima, Japan

Global Congress & Expo on Materials Science & Nanoscience
24-26 October 2016, Dubai, UAE

Precision Synthesis of Thiol-functionalized Polysaccharides by Phosphorylase-catalyzed Enzymatic Reaction

Taiji Jodoi, Kazuya Yamamoto, Jun-ichi Kadokawa

Abstract

Polysaccharides with reactive groups, such as carboxy, amino, and thiol groups, are expected as new functional materials. Especially, because a thiol group shows specific reactivity, thiol-functionalized polysaccharides have a potential to be applied as practical materials. On the other hand, because phosphorylase shows weak specificity for the recognition of substrates, it recognizes several analogue substrates of native one, i.e., α-D-glucose 1-phosphate (Glc-1-P), as glycosyl donors in glycosylations to give non-natural polysaccharides. For example, we have found that thermostable phosphorylase recognizes α-D-glucuronic acid 1-phosphate (GlcA-1-P) and α-D-glucosamine 1-phosphate (GlcN-1-P) as glycosyl donors in enzymatic glycosylations [1,2]. By means of these reactions, furthermore, amphoteric polysaccharides were synthesized using glucan dendrimer (GD), a highly branched glucan, as a glycosyl acceptor [3,4]. In this study, we investigated the phosphorylase-catalyzed enzymatic glucosylation using 6-deoxy-6-sulfanyl-α-D-glucose 1-phosphate (GlcS-1-P) as a new glycosyl donor and GD as a glycosyl acceptor to give a thiol-functionalized polysaccharide. The reaction was carried out in 2 : 1 donor / acceptor feed ratio in the presence of thermostable phosphorylase in acetate buffer (pH 6.2) at 55 °C for 15 h. The crude product was isolated by dialysis and its structure was determined by ^{1}H NMR spectrum.

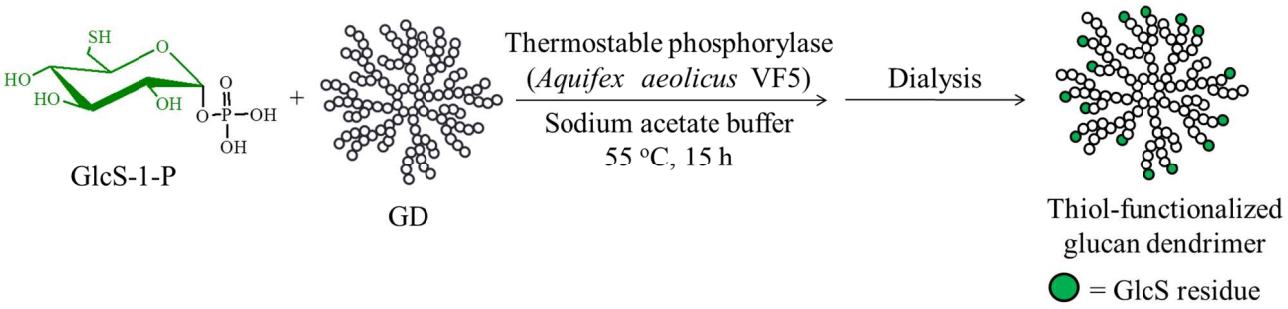

Scheme 1. Enzymatic synthesis of thiol-functionalized polysaccharide by thermostable phosphorylase-catalyzed glucosylation using GlcS-1-P as a glycosyl donor.

References

1) M. Nawaji, H. Izawa, Y. Kaneko, J. Kadokawa, *Carbohydr. Res.*, **2008**, *343*, 2692.
2) Y. Umegatani, H. Izawa, M. Nawaji, K. Yamamoto, A. Kubo, M. Yanase, T. Takaha, J. Kadokawa, *Carbohydr. Res.*, **2012**, *350*, 81.
3) Y. Takemoto, H. Izawa, Y. Umegatani, K. Yamamoto, A. Kubo, M. Yanase, T. Takaha, J. Kadokawa, *Carbohydr. Res.*, **2013**, *366*, 38.
4) Y. Takata, R. Shimohigoshi, K. Yamamoto, J. Kadokawa, *Macromol. Biosci.*, **2014**, *14*, 1437.

Department of Chemistry, Biotechnology, and Chemical Engineering, Graduate School of Science and Engineering, Kagoshima University, Kagoshima 890-0065, Japan

Global Congress & Expo on Materials Science & Nanoscience
October 24-26, 2016 Dubai, UAE

Precision Synthesis of Non-natural Heteropolysaccharides by Enzymatic Polymerization

Ryotaro Baba, Kazuya Yamamoto, Jun-ichi Kadokawa

Abstract

Phosphorylase catalyzes enzymatic polymerization of α-D-glucose 1-phosphate (Glc-1-P) as a monomer using a maltooligosaccharide as a primer to produce amylose with liberating inorganic phosphate [1, 2]. It was previously reported that α-D-glucosamine 1-phosphate (GlcN-1-P) and α-D-mannose 1-phosphate (Man-1-P) could be recognized as analogue substrates of Glc-1-P by potato phosphorylase in enzymatic α-glycosylations to give oligosaccharides having each residue at the nonreducing end. Because it is known that thermostable phosphorylase differs in recognition ability of substrates from potato phosphorylase, we found that the enzymatic polymerization of GlcN-1-P occurred when thermostable phosphorylase-catalyzed reaction was examined under the conditions of removal of inorganic phosphate as an ammonium magnesium phosphate precipitate in ammonia buffer including magnesium ion [3, 4]. On the basis of these backgrounds, in this study, we investigated the thermostable phosphorylase-catalyzed enzymatic copolymerization of Glc-1-P with Man-1-P to produce a non-natural α (1→4)-linked mannoglucan. The reaction was conducted using the maltotriose primer at 40 °C for 7 days in ammonia buffer including magnesium ion. The ^{1}H NMR and MALDI-TOF mass spectra of the isolated product supported the structure of mannoglucan (Figure). The molecular weights and Glc/Man unit ratios were depended on the monomer/primer feed ratios.

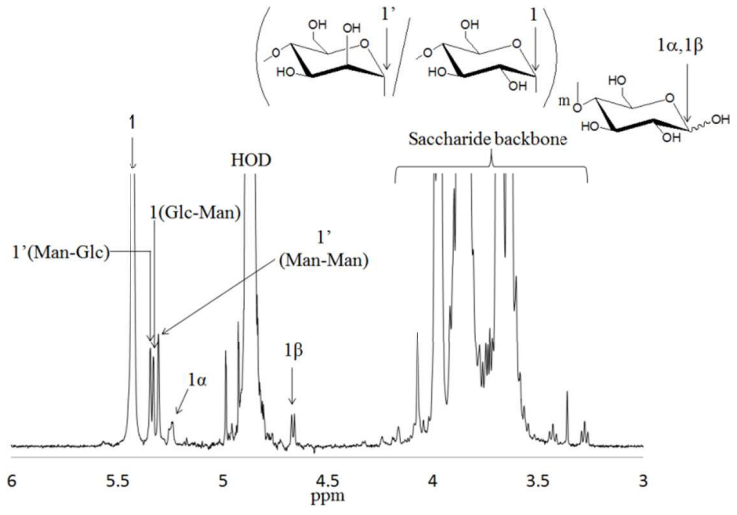

Figure. ^{1}H NMR spectrum of isolated product in D_2O

References

1. G. Ziegast, B. Pfannemüller, *Carbohydr. Res.*, **1987**, *160*, 185.
2. M. Kitaoka, K. Hayashi., *Trends Glycosci. Glycotechnol.*, **2002**, *14*, 35.
3. J. Kadokawa, R. Shimohigoshi, K. Yamashita, K. Yamamoto, *Org. Biomol. Chem.*, **2015**, *13*, 4336.
4. K. Yamashita, K. Yamamoto, J. Kadokawa, *Biomacromolecules*, **2015**, *16*, 3989.

Department of Chemistry, Biotechnology, and Chemical Engineering, Graduate School of Science and Engineering, Kagoshima University, Kagoshima 890-0065, Japan

Global Congress & Expo on Materials Science & Nanoscience
October 24-26, 2016 Dubai, UAE

Surface Modification and Material Processing of Self-assembled Chitin Nanofibers

Keisho Iimori, Ryo Endo, Kazuya Yamamoto, Jun-ichi Kadokawa

Abstract

Chitin is a natural aminopolysaccharide and an important renewable resource comparable to cellulose. However, it has been difficult to provide practical material applications from chitin, due to lack of solubility and processability. Derivatization of chitin is considered as one of the efficient methods for its materialization. Recently, we found that an ionic liquid of 1-allyl-3-methylimidazolium bromide (AMIMBr) dissolved or swelled chitin [1)], which was also used as a solvent for acetylation of chitin with acetic anhydride under mild conditions. Furthermore, we found that self-assembled chitin nanofiber film was obtained by regeneration from the chitin ion gel with AMIMBr using methanol, followed by filtration [2)]. In this study, we performed surface modification of the self-assembled chitin nanofibers by acetylation and their composite fabrication with commodity plastics, polyethylene. First, we prepared the self-assembled chitin nanofiber / DMF dispersion by regeneration from the chitin ion gel using methanol, followed by exchange of dispersion media to DMF. Surface acetylation of the products was performed by reaction with acetic anhydride for 12 h at r.t. in the dispersion. The resulting dispersion was subjected to filtration to obtain a partially acetylated chitin nanofiber film. The resulting film showed adhesive property with polyethylene. On the other hand, the original chitin nanofiber film didn't show adhesive property with polyethylene. Then, the composite with low density polyethylene was fabricated by pressing at 170 ^{o}C. The SEM measurement of the product observed the morphology that polyethylene covered nanofibers.

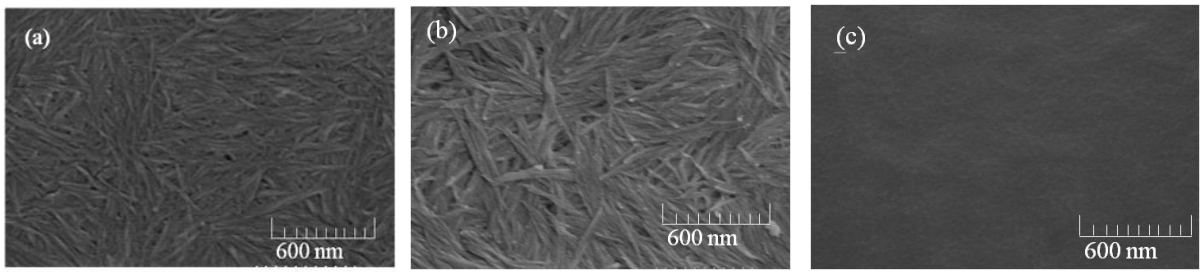

Figure. SEM images of chitin nanofiber film (a), partially acetylated chitin nanofiber film (b) and partially acetylated chitin nanofiber / polyethylene composite film (c)

Reference

1) K. Prasad, M. Murakami, Y. Kaneko, A. Takada, Y. Nakamura, J. Kadokawa, *Int. J. Biol. Macromol*., **45**, 221 (2009).
2) J. Kadokawa, A. Takegawa, S. Mine, K. Prasad, *Carbohydr. Polym.*, **84**, 1408 (2011).

Department of Chemistry, Biotechnology, and Chemical Engineering, Graduate School of Science and Engineering, Kagoshima University, Kagoshima 890-0065, Japan

The 29th International Symposium on Chemical Engineering, December 2-3, 2016,
Sheraton Grande Ocean Resort, Miyazaki, Japan

Effects of increase in volume of fluidizing gas on the bubble behavior of a bubbling fluidized bed

Hidekazu Miyata, Takami Kai, Tsutomu Nakazato

Abstract

The correlation of bubble size in fluidized beds has been actively studied to estimate the contact interface area in the past. However, these correlations are not adequately applied in the design of reactors [1]. One of the reasons is that all the correlations ignore the change in mole number, although many industrially useful reactions are accompanied with mole number change [2]. In this study, the water vapor evaporation method is used to expand the fluidizing gas volume. The effect of gas volume increase on the bubble behavior was examined base on the experimental data by distinguishing this effect from the change in gas and particle properties [3]. Assuming that the bubble eruption at the bed surface is a dominant factor of the pressure fluctuation, it is considered that the frequency of the pressure fluctuation represents the frequency of the bubble eruption and the deviation of the fluctuation reflects the bubble size. For this reason, the frequency and deviation of the pressure drop fluctuation were analyzed.

Fig. 1 shows the results of the wavelet transform of pressure fluctuations under the conditions of increase in gas volume and constant gas volume. Fig. 1 (a) and (b) were the results when the gas velocity was constant. The superficail gas velocity, U_G, was 4 cm/s for the former and 9 cm/s for the later. Although the intensity of the power of higher frequency decreased with increasing gas velocity, the wide distribution of the frequency intensity is observed in both the spectrum. Therefore, it is considered that the bubble size distribution shifted to the larger size. On the other hand, the intensity of the frequency larger than 7 Hz was hardly observed when gas volume increased as shown in Fig.1 (c). This is considered that the small bubbles disappeared.

When the gas volume increase was gradual, bubble size distribution was had equilibrium distribution. On the other hand, when the gas volume increase was rapid, the rate of bubble coalescence was higher than that of bubble splitting. Consequently, bubble size distribution shifted to larger size than equilibrium distribution at that gas velocity.

Reference

[1] Levenspiel, O., *Ind. Eng. Chem. Res.*, **47**, 273–277 (2008).
[2] Kai, T., J. Horinouch, T. Takahashi, *J. Chem. Eng. Japan*, **42**, s137–s141 (2009).
[3] Kai, T., S. Furusaki, *J. Chem. Eng. Japan*, **19**, 67–71 (1986).

Department of Chemical Engineering, Kagoshima University, Kagoshima 890-0065, Japan

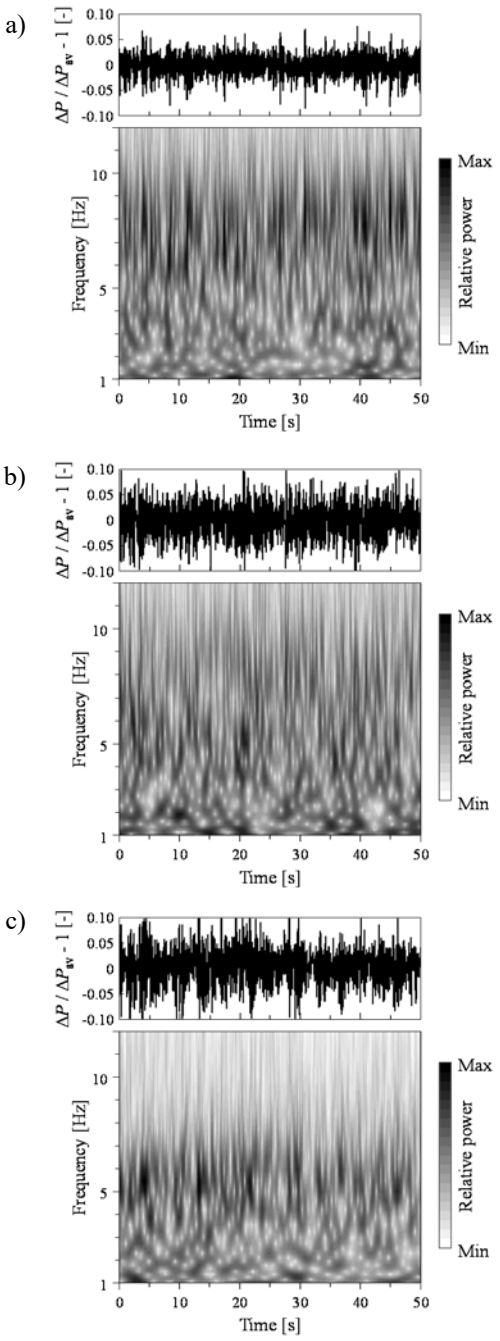

Fig. 1 Wavelet transform of pressure fluctuation signals: (a) U_G = 4.0 cm/s; (b) U_G = 9.0 cm/s; (c) U_{Gin} = 4.1 cm/s, U_{Gout} = 8.8 cm/s.

The 29th International Symposium on Chemical Engineering, December 2-3, 2016,
Sheraton Grande Ocean Resort, Miyazaki, Japan

Kinetic study of methylesterification of free fatty acids using ion-exchange resin catalysts

Midori Miyaji[1], Takami Kai[1], Tsutomu Nakazato[1], Saki Kobaru[2]

Abstract

Used cooking oils are the main raw materials for production of biodiesel fuel in Japan because of the high cost of fresh vegetable oils and effective use of resource. However, used cooking oils have large amounts of free fatty acids (FFAs). FFAs produce soap in reaction with alkali metal hydroxide. To prevent the soap formation, FFAs should be esterified using acid catalysts before the transesterification. Many reaction rate equations were proposed for the reactor design[1, 2] using ion exchange resins as catalysts. The relationship between the molar ratio of methanol/oleic acid and the conversion showed a characteristic trend[3]. It is required to elucidate this characteristic trend in order to derive the reaction rate equation. In addition, the reaction rate should be represented by the concentration of each component in the resin by considering the chemical equilibrium. The objective of this study is to establish the reaction rate over the ion exchange resins by these approaches.

In this study, molar ratios of methanol to oleic acid were changed. **Fig. 1** shows the effect of the ratio on the FFA conversion. The conversion increased with the ratio when it was below 10. It decreased and showed the lowest conversion at the molar ratio of 20. The conversion increased again when the ratio was above 20. The results indicate that the reaction rate was not simply affected by the concentrations of bulk liquid. The composition of the mixtures inside and outside of the resin must be different. Moreover, the relationship between them is probably complicated. **Fig. 2** shows the relationship between MeOH/FFA molar ratio and the reaction rate of FFA. It is clear that this relationship was not affected by the concentration of FFA in the oil phase. The change in the reaction rate can be divided into two curves. In the first curve, the conversion increased with the molar ratio and decreased after reaching the maximum point. In the other curve, the conversion increased with the molar ratio, and it approached asymptotically to a constant value. The volumetric fraction of methanol in the resin increased sharply with that in the bulk liquid phase. However, the volume ratio of methanol in the resin was almost constant and about 80% when the molar ratio MeOH/FFA was above 10. From the results described above, the following mechanism was considered. The reactions in the methanol phase and oil phase of the resins proceed with the different concentration dependency. Consequently, the characteristic trends shown in Figs. 1 and 2 were observed. Detailed analysis of the reaction rate will be conducted based on this mechanism.

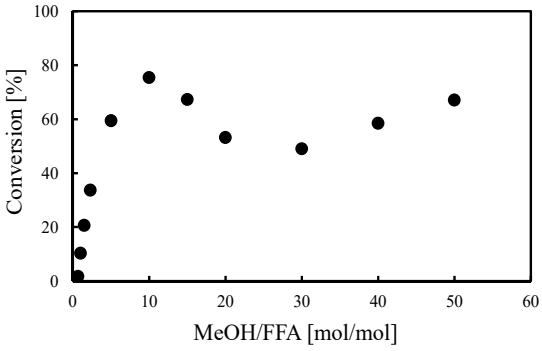

Fig. 1. Effect of molar ratio of methanol/oleic acid on the FFA conversion

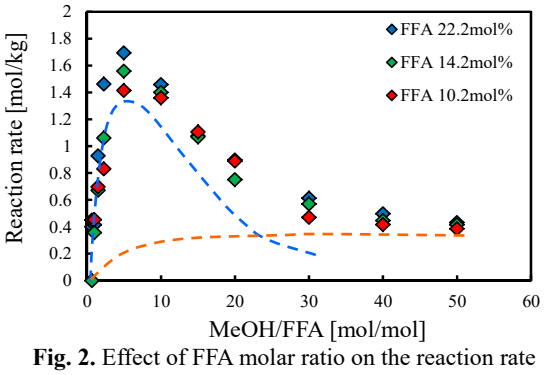

Fig. 2. Effect of FFA molar ratio on the reaction rate

References

1) Ilgen, O., *Fuel Proc. Technol.,* **124**, 134–139 (2014)
2) Tesser, R., L. Casale, D. Verde, M. D. Serio, E. Santacesaria, *Chem. Eng. J.,* **157**, 539–550 (2010)
3) Kai, T., H. Imafurukawa, T. Nakazato, H. Takanashi, K. Kusakabe, Abst. 45th SCEJ Autumn Meeting, Okayama, H126 (2013)

[1] Dept. of Chem. Eng., Kagoshima University, Kagoshima 890-0065, Japan
[2] Technical Sec., Grad. School of Sci. and Eng., Kagoshima University, Kagoshima 890-0065, Japan

The 29th International Symposium on Chemical Engineering, December 2-3, 2016,
Sheraton Grande Ocean Resort, Miyazaki, Japan

Biodiesel production from canola oil with DMC to reduce by-produced glycerol

Yuka Higashi[1], Takami Kai[1], Tsutomu Nakazato[1], Saki Kobaru[2]

Abstract

Some methods of glycerol free biodiesel production which used dimethyl carbonate (DMC) instead of methanol has been reported[1)]. Several methods of transesterification using DMC have been proposed[2, 3)]. When conventional alkali catalysts were used, it is required a large amount of catalysts or a high ratio of DMC to oils[4)] to achieve high conversion. The objective of this study is to reduce the amount of by-produced glycerol. For that purpose, the DMC-BDF production by the recrystallization of sodium methoxide catalyst[5)] is utilized. In this study, the methanol removal process is removed, and the amounts of methanol and the catalyst are reduced.

The conversion reached its maximum value after 60 min from the start of reaction independent of temperature. Although the initial reaction rate was increased with temperature, the conversion after 2 h was more than 80% for all temperature levels. Therefore, the effect of the amount of catalyst on the conversion was studied at relatively low temperature, 65°C. The added methanol molar ratio was 0.38. The effect of the amount of catalyst on the conversion is in **Fig. 1**. The conversion and FAME yield were above 80% and 60%, respectively when the amount of catalyst was above 0.35 wt%. Then the effect of the amount of methanol on the conversion was investigated. The conversion after 2 h reaction was showed in **Fig. 2**. The broken line is the calculated conversion of triglycerol reacted with methanol by the assumption that all the added methanol reacted with triglycerol. The conversion was below 1% without methanol addition. In contrast, the conversion increased drastically by adding methanol when the amount of catalyst was above 0.35 wt%. However, the conversion was not affected by the excessive quantity of methanol to dissolve catalyst completely. As the result, it is considered that the reaction rate was enhanced and high conversion can be obtained in the homogeneous system by adding minimum necessary amount of methanol on these reaction conditions. When the amount of catalyst was 0.35 wt%, the maximum conversion was below 85% even if the molar ratio of methanol to oil was 1.0. Judging from the results shown in Figs. 1 and 2, more than 0.5 wt% of the catalyst are necessary to obtain the conversion over 90%.

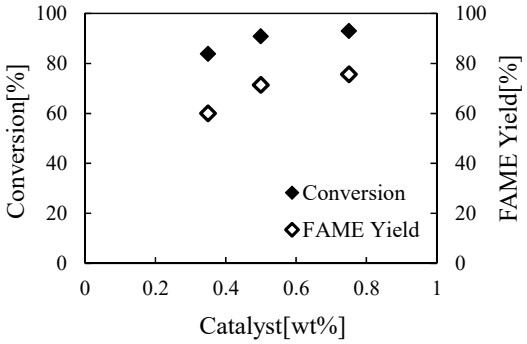

Fig. 1 Effect of amount of catalyst on the conversion and FAME yield

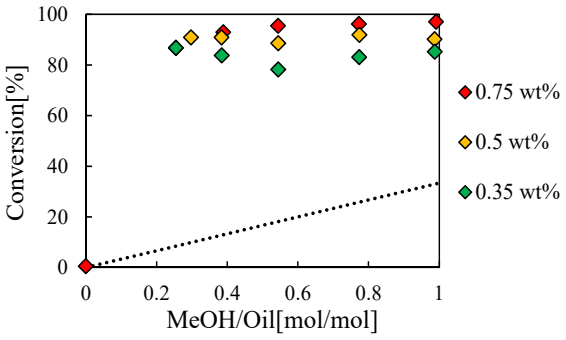

Fig. 2 Effect of molar ratio of MeOH to oil on the conversion after 2 h at 65°C

References

1) Fabbri, D., V. Bevoni, M. Notari, F. Rivetti, *Fuel*, **86**, 690–697 (2007)
2) Ang. G. T., K. T. Tan, K. T. Lee., *Renew. Sustain. Energy Rev*, **31**, 61–70 (2014)
3) Tan. K. T., K. T. Lee, A. R. Mohamed, *Fuel*, **89**, 3833–3839 (2010)
4) Zhang, L., B. Sheng, Z. Xin, Q. Liu, S. Sun, *Bioresourse Technol*., **101**, 8144–8150 (2010)
5) Kai, T., G. L. Mak, S. Wada, T. Nakazato, H. Takanashi, Y. Uemura, *Bioresource Technol*., **163**, 360–363 (2014)

[1] Dept. of Chem. Eng., Kagoshima University, Kagoshima 890-0065, Japan
[2] Technical Sec., Grad. School of Sci. and Eng., Kagoshima University, Kagoshima 890-0065, Japan

11th International Forum on Ecotechnology, Penang, Malaysia, December 25-26, 2016.

Production of titanium-calcium Hydroxyapatite photocatalyst powders via drip thermal treatment using a fluidized bed

Masaru Ketoguchi, Tsutomu Nakazato and Takami Kai

Abtract

Recently, hydroxyapatite (HAp; $Ca_{10}(PO_4)_6(OH)_2$), which has been used as artificial bone, adsorbent and catalyst, is receiving attentions in application to photocatalyst. Nishikawa [1] reported that UV irradiation after heat treatment at 200ºC leads to changes in the surface of HAp followed by the generation of the reactive oxygen species. Moreover, Wakamura *et al*. [2] have reported that the photocatalytic activity of HAp is enhanced by doping of Ti (IV). Further, the Ti (IV) doped HAp (Ti-HAp) has a higher bacterial effect than titanium dioxide (TiO_2) owing to superior ability for adsorption due to HAp. Kandori *et al.* [3] have reported that the photocatalytic activity of Ti-HAp is enhanced by heat-treatment at more than 600ºC.

From our previous study [4], Ti-HAp can also be produced from a scallop shell by properly selecting the conditions of post-heat treatment. This finding gives us an indication that post-heat treatment can be a crucial procedure for the improvement of photocatalytic activity of Ti-HAp. Until now, no studies have been found in the literature concerning Ti-HAp synthesis via drip thermal treatment using a fluidized bed (DTFB). The advantages of DTFB are the rapid evaporation of the solvent, effective heat treatment of the fine particles by attaching to the hot fluidizing coarse particles, prevention of the formation of aggregates and selective elutriation of heat-treated fine particles. Additionally, we believe that porous powders can be produced via DTFB.

The aim of this study is to explore the properties and photo-catalytic activity of Ti-HAp powders produced via DTFB. Our results indicated that, when $Ti(SO_4)_2$ are used as titanium source, $CaSO_4 \cdot 0.5H_2O$ is generated selectively. Although the photocatalytic activity was lower than that of commercially available photocatalytic apatite, careful washing of the suspension before the thermal treatment gave comparable photocatalytic activity to the commercial one.

References

1. H. Nishikawa; “Surface changes and radical formation on hydroxyapatite by UV irradiation for inducing photocatalytic activation,” *Journal of Molecular Catalysis A: Chemical*, **206**, 331-338 (2003)
2. M. Wakamura, K. Hashimoto and T. Watanabe; “Photocatalysis by Calcium Hydroxyapatite Modified with Ti(IV): Albumin Decomposition and Bactericidal Effect,” *Langmuir*, **19**, 3428-3431 (2003)
3. K. Kandori, M. Oketani, Y. Sakita and M. Wakamura; “FTIR studies on photocatalytic activity of Ti(IV)-doped calcium hydroxyapatite particles,” *Journal of Molecular Catalysis A: Chemical*, **360**, 54-60 (2012)
4. M. Ketoguchi, T. Nakazato and T. Kai; “Utilization of scallop shell for conversion to titanium-hydroxyapatite and its photocatalytic activity for acetaldehyde degradation,” 10th International Forum on Ecotechnology, Kagoshima, Japan (2015)

Department of Chemical Engineering, Kagoshima University, 890-0065, Kagoshima, Japan

The 31st International Congress of Psychology (ICP2016), July 24-29, 2016, Yokohama, Japan.

Length illusion on Benham's top

Kaori Shoji[1], Chiemi Miyata[1], Ken Kihara[1], Sakuichi Ohtsuka[1], Hiroshi Ono[2]

Abstract

Benham's top is known as the disk that observer perceives apparent color when it is spinning [1]. However, apparent color is not the focus of this study.

Our finding is that perceived length of the line segment is clearly enlarged only at the white-to-black transition on the white sector. When the disk is spinning, observers perceive that the front edge of black line segment at white-to-black transitions is elongated frontward.

In order to consider the perceptual mechanism, we examined length illusion in two ways; line segment length (Exp. 1) and endpoint location (Exp. 2). We employed real rotating disks instead of electronic displays in order to avoid the artifacts induced by frame refresh. The stimulus was rotated at 40 rpm (flicker frequency at 2Hz) in order to suppress blur as much as possible. Exp. 1 was magnitude estimation task by using static stimuli for comparison, and Exp. 2 was alignment task by using other rotating marks outside the disk. In both experiments, observers kept their gaze fixed in the middle of the disk, while directing their attention towards the line segment. Stimuli were employed three factors: line style (block, stripe), position of the line (rear, mid, front), and background color of the line (white, black).

Large difference in the results between Exps. 1 and 2 was observed only in the "rear / white-background" condition. Results of Exp. 1 showed that the line length was perceived clearly elongated in the "rear / white-back ground" condition (×1.4, Fig. 1A). And results of Exp. 2 showed that endpoint location was mostly correct at all positions. In order to obtain the length of a line segment, the locations of two endpoints should be given before. So, experiments show that the "line segment length (higher perceptual stage)" is perceived falsely in a particular case (Fig. 1B(a)) whereas the "endpoint alignment (lower perceptual stage)" is perceived mostly correct (Fig. 1B(b)). Therefore, we suggest that (1) this illusion occurs at a relatively high perceptual stage; length or shape not location, and (2) this phenomenon might indicate some visual system characteristic necessary for daily life.

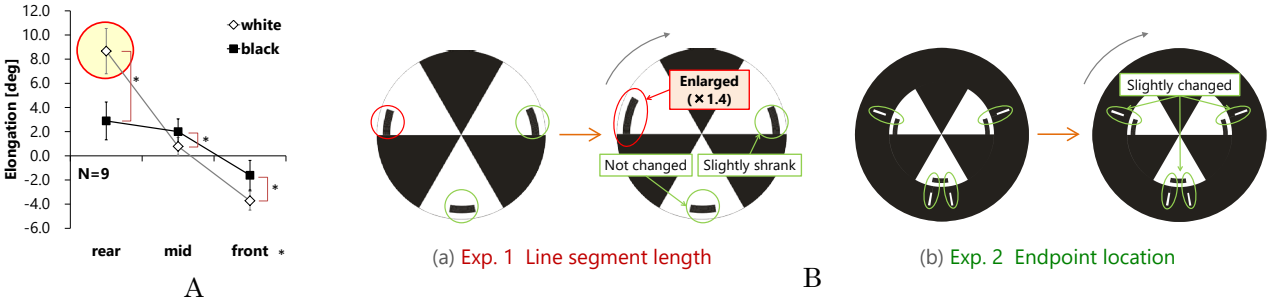

Figure. 1 Figures used in the poster.

References

1. C. von Campenhausen and J. Schramme, "100 years of Benham's top in colour science", Perception, vol.24, pp. 695-717, 1995.

[1] Department of Science and Engineering, Kagoshima University, 890-0065, Kagoshima, Japan
[2] Department of Psychology, York University, M3J-1P3, Toronto, Ontario, Canada

The 31st International Congress of Psychology (ICP2016), July 24-29, 2016, Yokohama, Japan.

Visual attention affects the fusional limit of a centrally located object when using an attentional blink task

Yuji Nosaki[1], Ken Kihara[1], Hiroshi Ono[2], Sakuichi Ohtsuka[1]

Abstract

Fusional limit is the maximum disparity at which we can fuse the retinal images of both eyes and perceive single vision (Fig.1A) [1]. The fusional limit is influenced by external factors (e.g., size of stimuli, retinal eccentricity) [2] [3]. However, the influence of internal factor (e.g., attention, training) on the fusional limit is unclear. To reveal a relationship between fusional limit and attention, we used attentional blink (AB) task where two targets (T1 and T2) are embedded among distractors, sequentially presented on the center of visual field (Fig.1B) [4]. In this task, the intensity of attention to T2 becomes higher when SOA is 100ms (i.e., T2 is presented just after T1), since the appearance of T1 enhances the attention. Also, when stimulus onset asynchrony (SOA) between two targets is 200-500ms, the intensity of attention to T2 becomes lower because of suppression by T1's following distractors. When SOA is 700ms, the intensity of attention recovers to a base level.

In this study, we measured the frequency of double vision when changing the intensity of attention by using a vertical line with disparities as T2 in AB task (Fig.1C). We created a line stimulus with various disparities using a stereoscopic 3D display (120Hz) and Liquid crystal shutter goggles. T1 was one of arrows (eight directions) and distractors were random octagons. T1 and distractors were not overlap a line stimulus. Participants were asked to identify arrow's direction and report line seemed single or double. We found that the frequency of double vision depended on SOA. Further, in AB task, we found that visibility of stimuli did not impact fusion process by an experiment which no item was presented after T2. The results of experiments showed that the higher intensity of attention decreased frequency of double vision (Fig.1D). These results suggest that paying attention to a centrally located object strengthens the fusion of binocular stimuli and increases the fusional limit.

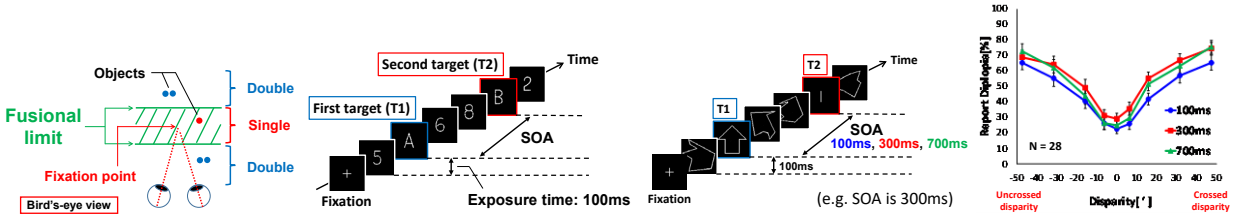

A B C D

Figure 1. Figures used in the poster.

References

1. I. P. Howard, "Binocular fusion and rivalry", *Seeing in Depth Volume I Basic Mechanisms*, Toronto, pp. 271-315, 2002.
2. D. E. Mitchell, "Retinal disparity and diplopia", Vision Research, Vol. 6, no. 7-8, pp. 441-451, 1966.
3. D. A. Palmer, "Measurement of the horizontal extent of Panum's area by a method of constant stimuli", Optica Acta, Vol. 8, no. 2, pp. 151-159, 1961.
4. J. E. Raymond, K-L. Shapiro, and K-M. Arnell, "Temporary suppression of visual processing in an RSVP task: An attentional blink?", Journal of Experimental Psychology, Vol. 18, pp. 849-860, 1992.

[1] Department of Science and Engineering, Kagoshima University, 890-0065, Kagoshima, Japan
[2] Department of Psychology, York University, M3J-1P3, Toronto, Ontario, Canada

2016 International Symposium on Radio-Frequency Integration Technology, August 24-26, 2016, Taiwan

Design of Dual-Band Rectifier Using Microstrip Spurline Notch Filter

Koshi Hamano[1], Ryuya Tanaka[1], Satoshi Yoshida[1], Akihira Miyachi[2],

Kenjiro Nishikawa[1], and Shigeo Kawasaki[2]

Abstract

This paper proposes and demonstrates a novel dual- band rectifier at 2.45 GHz and 5.8 GHz. The proposed rectifier employs a microstrip spurline notch filter to realize dual-band high RF-DC conversion efficiency. The control of reflected signals from the output filter to maximize the voltage swing at the diode, and use of the spurline notch filter provide high-level conversion efficiencies at both operating frequency bands. The fabricated proposed dual-band rectifier achieves the RF-DC conversion efficiencies of 55.9 % and 55.4 % at 2.15 GHz and 5.84 GHz, respectively. These results are top-level performances of the dual- band rectifiers.

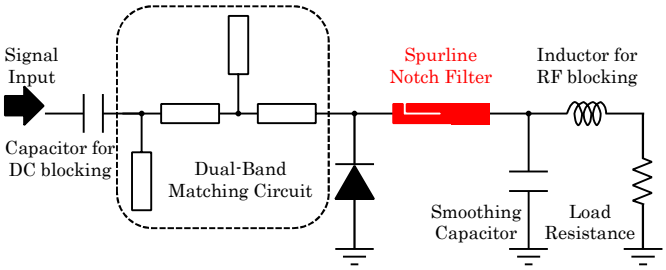

Fig. 1. Schematic of dual-band rectifier.

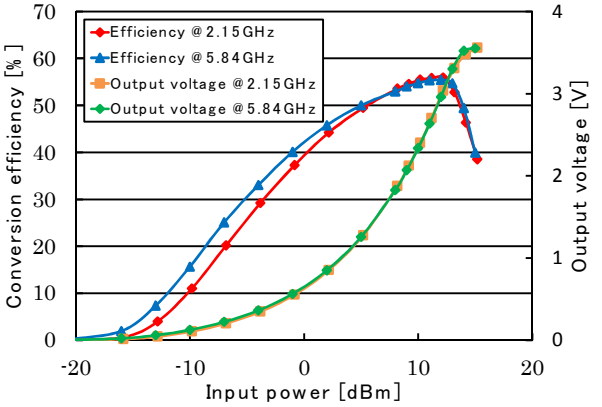

Fig. 2. RF-DC conversion efficiency comparison of reported dual-band rectifiers.

REFERENCES

[1] S. Kawasaki, "Wireless Communication/Energy Transmission and RF Energy Harvesting," The Journal of Institute of Electronics, Information and Communication Engineers, Vol. 95, No. 9, pp.815-822, Sept. 2012 (in Japanese).

[2] J. Heikkinen, M. Kivikoski, "A Novel Dual-Frequency Circularly Polarized Rectenna," IEEE Antennas and Wireless Propagation Letters, Vol. 2, pp. 330-333, 2003.

[3] H. Sun, Y.-X. Guo, M. He, Z. Zhong, "A Dual-Band Rectenna Using Broadband Yagi Antenna Array for Ambient RF Power Harvesting," IEEE Antennas and Wireless Propagation Lett., Vol. 12, pp. 918-921, 2013.

[4] K. Niotaki, S. Kim, S. Jeong, A. Collado, A. Georgiadis, M. M. Tentzeris, "A Compact Dual-Band Rectenna Using Slot-Loaded Dual Band Folded Dipole Antenna," IEEE Antenna and Wireless Propagation Lett., Vol. 12, pp. 1634-1637, 2013.

[5] H. Takhedmit, L. Cirio, Z. Saddi, J. D. Lan Sun Luk, O. Picon, "A Novel Dual-Frequency Rectifier based on a 180° Hybrid Junction for RF Energy Harvesting," EuCap 2013, pp.2472-2475, April 2013.

[6] D. Wang, R. Negra, "Design of a dual-band rectifier for wireless power transmission," 2013 IEEE Wireless Power Transfer, pp.127-130, May 2013.

[7] J. A Hagerty, F. B. Helmbrecht, W. H. McCalpin, R. Zane, Z. B. Popovic, "Recycling Ambient Microwave Energy with Broad-Band Rectenna Arrays," IEEE Trans. On Microwave Theory and Techniques, Vol. 52, No. 5, pp. 1548-1553, May 2003.

[1]Dept. of Electrical and Electronics Engineering, Kagoshima University, Japan
[2]Institute of Space and Astronautical Science, Japan Aerospace Exploration Agency, Japan

The 33rd International Korea-Japan Seminar on Ceramics, Daejeon, Korea, Nov. 16-19, 2016.

Performance of Yttria-stabilized Zirconia Fuel Cell using CO–O_2 Gas System and H_2O Gas as an Oxidant

Yoshihiro HIRATA*, Shinji DAIO**, Ayaka KAI***, Taro SHIMONOSONO****, Reiji YANO**, Soichiro SAMESHIMA*****, Katsuhiko YAMAJI******

Abstract

The performance of an yttria-stabilized zirconia fuel cell (YSZ) was examined using CO-O_2 gas system and H_2O oxidant gas.[1] The final target of this research is to establish the combined fuel cell systems which can produce a H_2 fuel and circulate CO_2 gas in the production process of electric power. Fig.1 shows two types of the combined reaction systems for the production of H_2 fuel and the circulation of CO_2 gas in the production process of electric power. A large electric power was measured in the H_2–O_2 gas system and the CO–O_2 gas system at 1073 K (Fig.2). The formation process of O^{2-} ions in the endothermic cathodic reaction ($1/2O_2 + 2e^- \rightarrow O^{2-}$) controlled the cell performance. The CO–H_2O gas system and the H_2–H_2O gas system was expected to produce a H_2 fuel in the cathode ($CO + H_2O \rightarrow H_2 + CO_2$, $H_2 + H_2O \rightarrow H_2 + H_2O$). Although relatively high OCV values (open circuit voltage) were measured in these gas systems, no electric power was measured. At this moment, it was difficult to apply H_2O vapor as an oxidant to the cathodic reaction in a YSZ fuel cell.

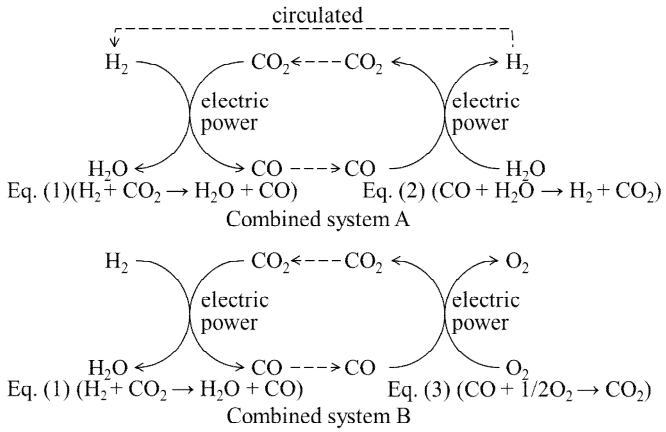

Fig. 1 Combined reaction systems for the production of a H_2 fuel and the circulation of CO_2 gas in the production process of electric power.

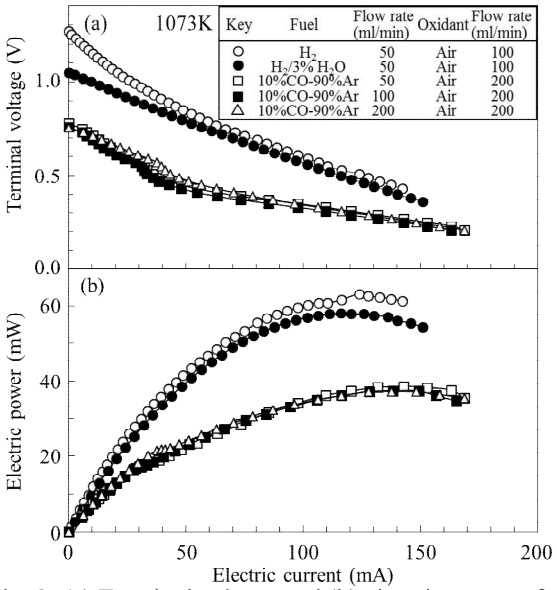

Fig. 2 (a) Terminal voltage and (b) electric power of a YSZ cell using the H_2–O_2 gas system and the CO–O_2 gas system at 1073 K.

References

1) Y. Hirata, S. Daio, A. Kai, T. Shimonosono, R. Yano, S. Sameshima and K. Yamaji, "Performance of yttria-stabilized zirconia fuel cell using H_2–CO_2 gas system and CO–O_2 gas system", Ceramics International, Vol. 42, pp. 18373-18379, 2016.

*Professor, **Graduate Student, ***Undergraduate Student, ****Assistant Professor, *****Associate Professor, Department of Chemistry, Biotechnology, and Chemical Engineering

******Group Leader, Fuel Cell Materials Group, Research Institute for Energy Conservation, National Institute of Advanced Industrial Science and Technology

The 31st International Congress of Psychology (ICP2016), July 24-29, 2016, Yokohama, Japan.

The role of the locus coeruleus-noradrenaline system in attention on visual change detection: a pupillometric study

Hijiri Kodama[1], Ken Kihara[1], Sakuichi Ohtsuka[1]

Abstract

Humans sometimes fail to notice obvious changes in objects in the field of view when the changes are unexpected. Failure to discern the change occurs because the object was not being attended to. This phenomenon is known as change blindness (Fig.1A). It is suggested that the activity of the locus coeruleus-noradrenaline (LC-NA) system is involved in regulating attention [1]. Therefore, in this study, we investigated the temporal dynamics of LC-NA system activity in attention during the periods before and after change detection.

We used a change detection task. Stimuli changes in 15 seconds. We repeatedly presented stimulus until participant could detect the change at a maximum of 10 attempts. Participants press the key as quickly as possible when they detect a change. This study uses measured pupil diameter during change detection task, because pupil changes directly reflect LC neuron activity [2]. We presented two types of stimuli, because we investigate influence on change detection by the context. Experiment 1 was change detection of natural scenes, and experiment 2 was change detection of geometric figures.

As a result, Pupil dilation was observed before the detection of the change (Fig.1B). We also found that the results of experiment 2 using geometric figures replicated those of experiment 1 using natural scenes.

These results suggest that the activity of the LC-NA system mediates attentional orientation to changing visual objects before awareness of the changes (Fig.1C). Firstly, pre attentive visual processing can find a changing area roughly by comparing past scene with present scene. Next, LC-NA system is activated, which enhances and orients attention to the location of the change. We then consciously detect the change. The activation of the LC-NA system for the change detection does not depend on types of the changing object.

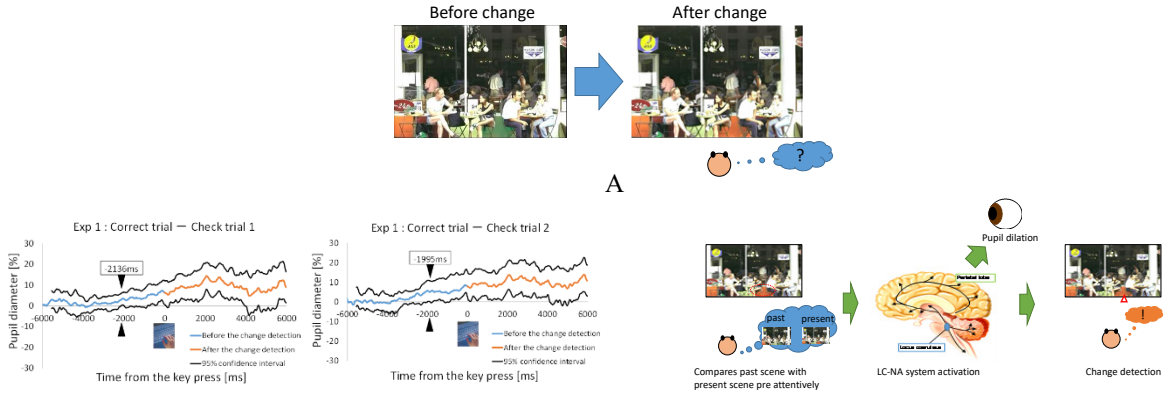

Figure.1 Figures used in the poster.

References

1. B. Laeng, S. Sirois, G. Gredeback, “Pupillometry: A Window to the Preconscious?”, Perspectives on Psychological Science, vol. 7, No. 1, pp. 18-27, 2012.
2. Gary Aston-Janes, Jonathan D. Cohen, “An Integrative Theory of Locus Coeruleus-Norepinephrine Function: Adaptive Gain and Optimal Performance”, Annu. Rev. Neurosci., vol. 28, pp.403-450, 2005.

[1] Department of Science and Engineering, Kagoshima University, 890-0065, Kagoshima, Japan

Neurophysiological Evaluation of Visual and Haptic Sense Mechanisms in Grip Movements with Artificial Visual Transmission Delay

Yasushi Fujiwara, Kazutomo Yunokuchi, Atsuo Maruyama, Atsuo Nuruki

Abstract

Prior studies have been performed about weight illusions showing that grip movements can manipulate visual feedback. However, in these experiments, usually only the appearance of the object is changed, such as in the Material-Weight Illusion (MWI) or Size-Weight Illusion (SWI), the most famous among the weight illusions. Here, we confirm the phenomenon of the weight illusion being induced by creating a temporal difference between an object's motion information (lifting) and its visual information (lifted). We used here a virtual reality device with a stereoscopic object gripping system using two haptic devices. We show that it was the manipulation of time that caused the illusion. Still, we could observe neither change of grip force (GF) nor load force (LF) in grip movements of the participants.

Using transcranial magnetic stimulation (TMS), we investigated the activity of the primary motor cortex by examining the excited state of this area during presentation of a visual transmission delay. We observed that the amplitudes of motor evoked potentials were different between various transmission delay times. This result suggests that the weight illusion is associated with activation of the motor cortex and not muscle activity.

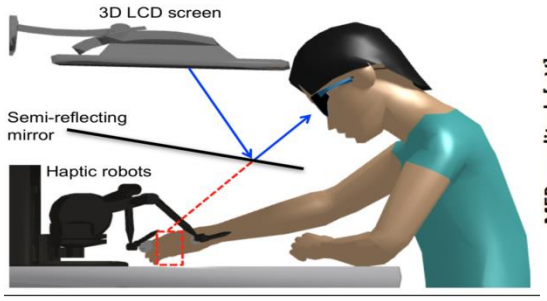

Fig.1 : Stereoscopic and Gripping System

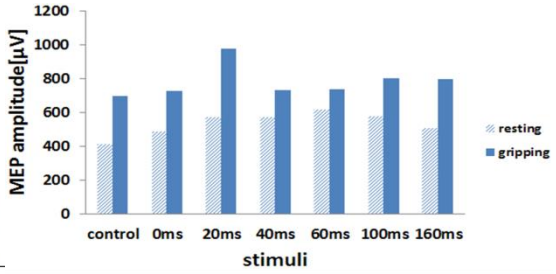

Fig.7 : MEP amplitude (subject1)

References

1. Kinoshita H, Kawai S, Ikuta K. : "Contributions and coordination of individual fingers in multiple finger prehension", Ergonomics, Vol.35, No.3, pp.1212-1230 (1995)

2. Radwin R. G., Oh S., Jensen T. R., Webster J. G. : "External finger forces in submaximal five finger static pinch prehension", Ergonomics, Vol.35, No.3, pp. 275-288 (1992)

1 Graduate School of Science and Engineering, Kagoshima University, 890-0065, Kagoshima, Japan

2 Health Sciences, Niigata University of Health and Welfare, 950-3102, Niigata, Japan

8th International Workshop on Biosignal Interpretation, November 1-3,2016, Osaka, Japan

The relationship between recovery from muscle fatigue of the skeletal muscle and magnetic stimulation

Yuya Yokota, Kazutomo Yunokuchi, Atsuo Nuruki

Abstract

Muscle fatigue is common in everyday life and sports. Magnetic stimulation therapy is known to be effective for early recovery from muscle fatigue. However, the mechanism is still unknown. In order to clarify the mechanism of magnetic stimulation effect on muscle fatigue, we performed magnetic stimulation on the muscle during isometric contraction for fourteen normal adult males. The load strength of the exercise assumed 30% and 60% maximum voluntarily contraction (MVC). Moreover, exercise performance was evaluated using an electromyography analysis technique under two conditions: use and non-use of magnetism stimulation. No significant difference was observed between the two conditions regardless of load strength. In a previous study, an improvement in exercise performance was observed when magnetic stimulation was applied to a resting muscle after an exercise with 60% MVC. Careful assessment of the physiological difference between resting and exercising reveals possible differences in energy consumption. In order to this difference, it might occur for the recovery effect difference by the magnetic stimulation.

		60% MVC (n=10)			30% MVC (n=4)		
		Endurance time [s]	Rate of change of iEMG [%/seg]	Rate of change of MPF [%/seg]	Endurance time [s]	Rate of change of iEMG [%/seg]	Rate of change of MPF [%/seg]
Magnetic Stimulation	With-out	59.15	+1.699	-0.712	225.3	+0.250	-0.700
	With	52.13	+2.342	-0.758	244.7	+0.898	-0.825
Significant difference (p<0.05)		Non	Non	Non	Non	Non	Non

Table 1: Results of the experimentation

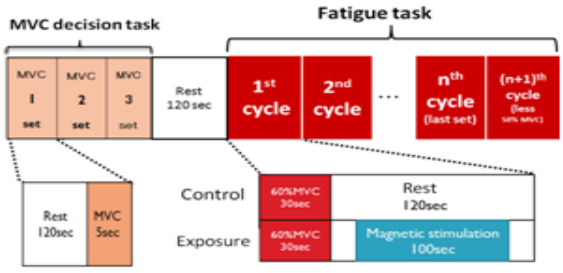

Fig 1: Experimental protocol of our previous study

References

1. Komiyama T, Kawai T, Furubayashi T: Neurophysiological basis of muscle fatigue, Chiba University,42:2, 1994
2. Oda T, Nuruki A, Yunokuchi K: Recovery Effect of the muscle fatigue by the Pulse Magnetic Stimulation, The institute of electrical engineers of japan-Study Group document, Vol.MAG-13, No.1-4.6-14:27-31, 2013

Depertment of Information Science and Biomedical Engineering Faculty of Engineering, Kagoshima University, Japan